Title	Anisotropic oxide ion conduction in melilite intermediate temperature electrolytes
Author(s)	Wei, Fengxia; Gasparyan, Hripsime; Keenan, Philip J.; Gutmann, Matthias; Fang, Yanan; Baikie, Tom; Claridge, John B.; Slater, Peter R.; Kloc, Christian Leo; White, Timothy John
Citation	Wei, F., Gasparyan, H., Keenan, P. J., Gutmann, M., Fang, Y., Baikie, T., et al. (2015). Anisotropic oxide ion conduction in melilite intermediate temperature electrolytes. Journal of Materials Chemistry A, 3(6), 3091 -3096.
Date	2015
URL	http://hdl.handle.net/10220/39743
Rights	© 2015 The Royal Society of Chemistry. This is the author created version of a work that has been peer reviewed and accepted for publication by Journal of Materials Chemistry A, The Royal Society of Chemistry. It incorporates referee's comments but changes resulting from the publishing process, such as copyediting, structural formatting, may not be reflected in this document. The published version is available at: [http://dx.doi.org/10.1039/C4TA05132G].

Graphic Abstract

Anisotropic Oxygen Ion Conduction in Melilite Intermediate Temperature Electrolytes

Fengxia Wei, Hripsime Gasparyan, Philip Keenan, Matthias Gutmann, Yanan Fang, Tom Baikie, John B. Claridge, Peter Slater, Christian Kloc, Tim White*

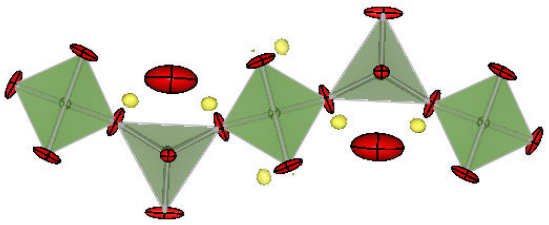

Melilite, a tetrahedral-layered structure, shows strong anisotropic oxygen ion conduction at intermediate temperatures, which can be controlled by increasing the number of interstitial oxygen and reducing the size of interlayer cations.

Anisotropic Oxide Ion Conduction in Melilite Intermediate Temperature Electrolytes

Fengxia Wei,[a, f] Hripsime Gasparyan,[b] Philip Keenan,[c] Matthias Gutmann,[d] Yanan Fang,[a] Tom Baikie,[e] John B. Claridge,[b] Peter Slater,[c] Christian Kloc,[a] Tim White[a*]

[a] Division of Materials Science & Engineering, Nanyang Technological University, Singapore.
[b] Department of Chemistry, University of Liverpool, United Kingdom.
[c] School of Chemistry, University of Birmingham, United Kingdom.
[d] Rutherford Appleton Laboratory, ISIS Facility, Chilton Didcot, Oxfordshire OX11 0QX, United Kingdom.
[e] Energy Research Institute @ NTU (ERI@N), Research Technoplaza, Nanyang Technological University, Singapore
[f] Advanced Materials Technology Centre, Department for Technology, Innovation and Enterprise, Singapore Polytechnic, 500 Dover Road, Singapore

Abstract

Electrolytes with oxide ion conductivities higher than 10^{-2} Scm^{-1} at moderate temperatures (~ 500 - 900 °C) offer the possibility for solid oxide fuel cells to operate with less maintenance. This study of $[A_{1+x}B_{1-x}]_2[Ga]_2[Ga_2O_{7+x/2}]_2$ ($0 \leq x \leq 0.5$) (A = La, Nd, B = Ca, Sr) layered-melilite found that in large single crystals intralayer oxide ion conduction is dominant. This anisotropic behavior arises by relaxation about the interstitial oxygen through changes in the interlayer A and Ga coordination, and at 850°C conductivity is ~0.008 Scm^{-1} along the ***c*** direction and ~0.036 Scm^{-1} perpendicular to the ***c*** axis. It is found that the ionic conductivity can be optimized by increasing the number of interstitial oxygen and reducing the size of interlayer cations.

Keywords: anisotropic oxide ion conduction, electrolyte, structure-property relation

1. Introduction

The drive towards sustainable energy production and conservation supports the expansion of fuel cell technologies, especially solid oxide fuel cells (SOFC), due to their high efficiency, long-term stability, low emissions, fuel flexibility and economic running costs. SOFC have three basic components – the porous anode, ion-conducting electrolyte and porous cathode[1] – with energy conversion efficiencies for ceramic fuel cell up to 60% and cell output of 100kW.[2] However, the high operating temperature of conventional SOFCs results in long start-up times and mechanical/chemical incompatibility that can lead to structural failures. One approach to overcome these disadvantages is to deploy electrolytes having significant oxide ion conductivity at moderate temperatures (< 800°C), negligible electronic conductivity, good chemical stability, and a coefficient of thermal expansion compatible with the anode and cathode. [1]

In conventional electrolytes, ionic transport is mediated by oxygen vacancies, with the mechanisms in perovskite-[3] and fluorite-type[4] oxides well understood. However, electrolytes functionalized by interstitial oxygen diffusion, as found in certain apatites[5] and fergusonites, [6] are of growing interest due to their relatively lower activation energies for migration and possibly higher oxide ion conductivities at reduced temperatures. Another crystal family known to accommodate a large interstitial oxide ion concentration are the melilite-type compounds.[7] For example, $[Ca_{0.36}La_{1.64}]_2[Ga]_2[Ga_2O_{7.32}]_2$ melilite containing up to 0.32 superstoichiometric oxygen per formula unit, achieved an ionic conductivity 0.02-0.1 Scm^{-1} at 600-900°C,[7] that is well in excess of 0.04-0.16 Scm^{-1} from 800-950°C for benchmark yttria (8mol%) stabilized zirconia(YSZ) over a smaller temperature range.[8] In general, the passage of interstitial oxygen requires 1D tunnels or 2D layering that can flex and provide a migration pathway that satisfies bond length and bond valence criteria; apatites,[5] fergusonites[6] and melilites[9] all exhibit this adaptation.

Melilites adopt tetragonal $P\bar{4}2_1m$ symmetry, and have the general formula $[A_2]_2[B^{I}]_2[B^{II}{}_2O_7]_2$ where A are large divalent or trivalent ions (e.g. *Ln*, Ca, Sr and Ba) and B^{I}, B^{II} are symmetrically distinct small cations (e.g. Si, Ga and Ge). In melilite, the corner-connected tetrahedra form two-dimensional layers, between which large cations A are located. Many compositions are incommensurately modulated, including the gallate melilites that are promising intermediate temperature SOFC electrolytes.[9-10] This study focuses on the facilitation of oxygen diffusion through structural modulation in this family of electrolytes.

2. Experimental Details

Synthesis. Precursor powders (10 grams) containing a stoichiometric mixture of La_2O_3 (99.998% Alfa Aesar), $CaCO_3$ (99.9%, Alfa Aesar) and Ga_2O_3 (99.999%, Aldrich) were ground and homogenized in ethanol, dried in air (100°C/6 hours), then fired (800°C/10 hours) to decompose $CaCO_3$. The La_2O_3 was dehydrated and decarbonated (1000°C/10 hours) before use. The calcines were reground, pressed into pellets (for powder analysis) or two rods (that served as feed and seed rods for single crystal growth) and sintered (1400 °C/12 hours/air) to yield single phase products. Single crystals of $[Ca_{1-x}La_{1+x}]_2[Ga]_2[Ga_2O_{7+x/2}]_2$ ($0 \leq x < 0.6$) were grown using an optical floating zone furnace, with growth speed ~ 0.1 to 1 mm/hour in air (Figure S1).

Single crystal X-Ray diffraction. A single crystal (0.1mm×0.1mm×0.08mm) was cleaved and mounted on a glass fibre. Data were collected using a Bruker Smart Apex II single crystal diffractometer (X-ray radiation Mo $K\alpha$, λ=0.71073Å), over an angular range of $2.08° \leq \theta \leq 37.84°$, with an exposure time of 30s (step size 0.5 degree) to give a total collection time of ~7 hours. The Saint module, deployed within Apex II, was used for reflection

integration, performing Lorentz polarization and multi-scan absorption corrections. The data were analyzed using JANA2006[11] and no extra absorption correction was applied.

Single crystal neutron diffraction. Measurements were carried out at the single crystal diffractometer SXD instrument installed at the ISIS pulsed neutron source,[12] with an array of two-dimensional position-sensitive detectors. This neutron time-of-flight Laue technique can measure diffraction data through a very large volume of reciprocal space. A single crystal was fixed on an aluminium pin with adhesive Al tape and mounted on a closed-cycle refrigerated holder. Measurement was conducted at room temperature, and structure determination was carried out using JANA2006.

Powder X-ray diffraction (PXRD). Patterns were collected on a Bruker Advance D8 X-ray diffractometer operated at 40 kV and 40 mA. The powders were mounted onto a top-loaded holder and data collected from 2θ 5-130° using a step size of 0.02° with an exposure time 1s per step. Rietveld refinement was applied using TOPAS V4.1.[13]

Scanning electron microscopy. Polycrystalline pellets were examined by secondary electron images (SEI) obtained with a scanning electron microscope (JEOL 5410) equipped with an energy dispersive X-ray (EDX) operating at 10-15 keV. To remove excess charge, the samples were gold sputter coated before attaching with double sided carbon tape to an aluminum stage.

Transmission electron microscopy (TEM). Single crystals were crushed under ethanol and deposited on holy carbon films supported by a copper grid. High resolution image (HRTEM) and select area diffraction pattern (SAED) were collected using JEOL 2100F operated at 200 kV and fitted with a Gatan Ultra CCD camera.

Impedance spectroscopy. For the conductivity measurements of the polycrystalline pellets of $[La_{1+x}Ca_{1-x}][Ga]_2[Ga_2O_{7+x/2}]_2$ ($0.1 \leq x \leq 0.6$), the pellets were coated on both sides with Pt paste, and then heated to 800° C for 1 hour to ensure bonding to the electrolyte. Ionic conductivities were measured by alternating current (AC) impedance spectroscopy (Hewlett Packard 4182A impedance analyzer) attributed to oxide ions to examine the response when applying a small AC potential to a cell as a function of frequency. The experiments were conducted from 500 to 800°C in air at an applied AC voltage of 0.1 V from 5 Hz to 13 MHz. Since it was not possible to separate bulk and grain boundary semicircles, the data reported represent total conductivities. Single crystals were cut into disks, with Au paste coated onto both sides, and then heated to 750°C to ensure bonding, using a procedure commonly applied to polycrystalline ceramic pellets.[14] The experiments for single crystals were conducted from 600 to 850°C in air at an applied AC voltage of 10m V from 100 mHz to 400 KHz.

3. Results and Discussions

The polycrystalline pellets $[Ca_{1-x}La_{1+x}]_2[Ga]_2[Ga_2O_{7+x/2}]_2$ ($0 \leq x < 0.6$), with phase homogeneity confirmed by PXRD (Figure S4), show ~ 92% theoretical density with grain morphology examined by scanned secondary electron images (SEI) (Figure S5). The preferred crystal growth direction was determined to be along the crystallographic ***c*** axis through electron backscatter diffraction (EBSD) on the seed crystal (Figure S6). The EBSD also shows the crystals are not strictly single crystalline with domains slightly tilted (maximum 3°) away from principal axis. The structural information for $[La_{1+x}Ca_{1-x}]_2[Ga]_2[Ga_2O_{7+x/2}]_2$ ($0 \leq x \leq 0.5$) is also provided in the supporting information. Strong anisotropic elongations for oxygen in these structures appear due to the misfit between the size of interlayer cations and interlayer space.[9]

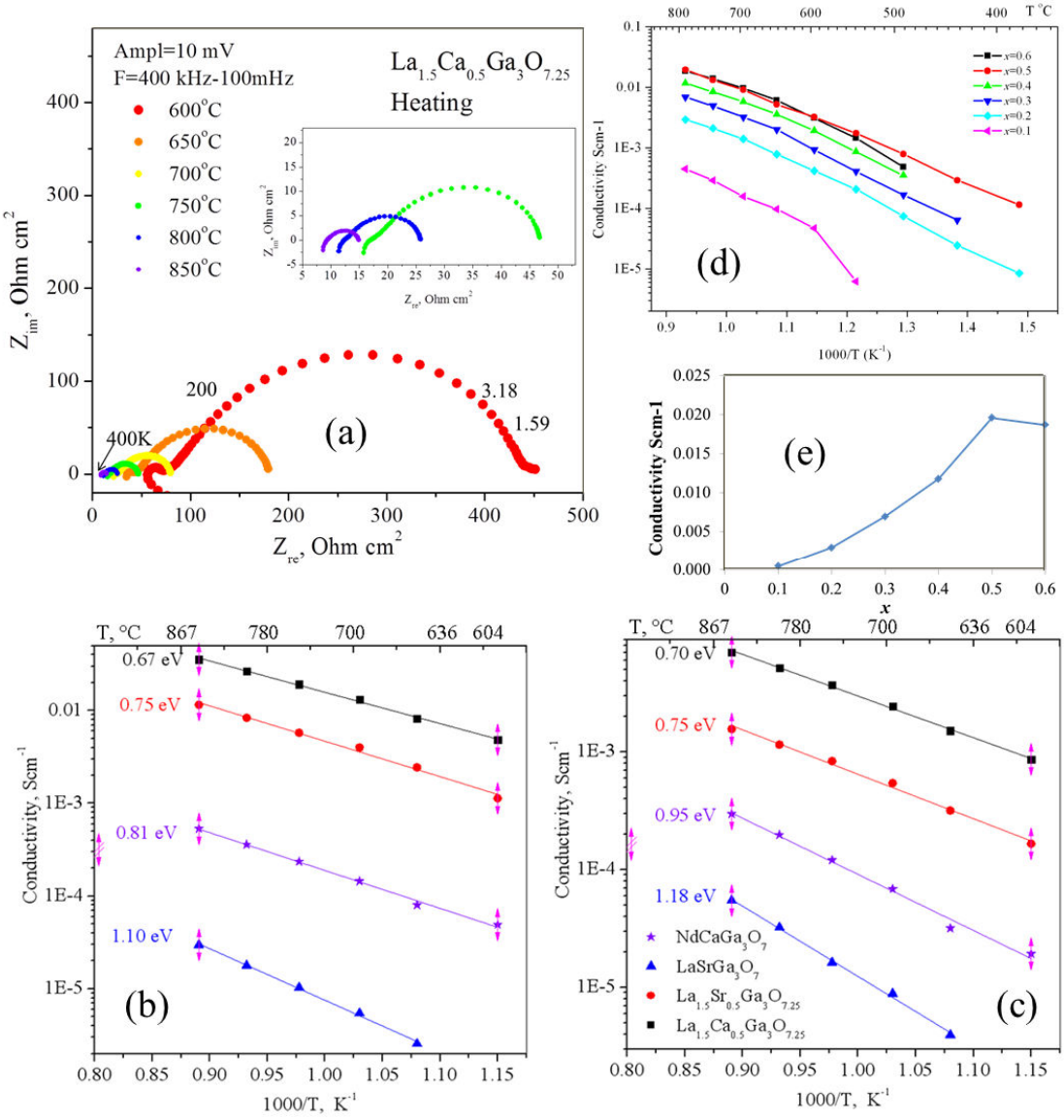

Figure 1. (a) Complex impedance plot for single crystal $[La_{1.5}Ca_{0.5}]_2[Ga]_2[Ga_2O_{7.25}]_2$ perpendicular to ***c*** axis. (b) Strong anisotropic ionic conduction is shown for melilite single crystals perpendicular to *c* and (c) along *c* direction. (d) Ionic conductivity of $[La_{1+x}Ca_{1-x}][Ga]_2[Ga_2O_{7+x/2}]_2$ ($0.1 \leq x \leq 0.6$) pellets. (e) The conductivity as a function of *x* at 800°C.

Oxide ion conductivities were measured by Impedance Spetroscopy (IS) attributed to oxide ions. Figure 1a shows in the form of complex impedance plots (Nyquist) open-circuit impedance spectra corresponding to the $[La_{1.5}Ca_{0.5}]_2[Ga]_2[Ga_2O_{7.25}]_2$ single crystal which

consists of 2 partially overlapping semicircles. The smaller semicircle at high frequencies which corresponds to electrolyte's bulk conductivuty gradually disappears with increasing temperature due to strong overlapping with larger semicircle appearing at lower frequencies that is associated with electrode-electrolyte interface. Low frequency arc corresponds to the electrode respond (dispersion) and calculated capacitances for low frequency arc are in order of C_{LF}~7E-5 F/cm^2 for this sample. Conductivity values were calculated from the ohmic resistances that were obtained from the equivalent curcuit fittings of the experimental data having into account electrolytes geometric parametres (Table S2).

Anisotropic ion transport. The impedance spectroscopy for all melilite single crystals shows strong anisotropic ion conduction (Figure 1b and 1c), e.g. the high ionic conductivity of ~ 0.036 Scm^{-1} at 850 °C for $[La_{1.5}Ca_{0.5}]_2[Ga]_2[Ga_2O_{7.25}]_2$ perpendicular to ***c*** axis ($\sigma\perp$) is comparable to YSZ, but is only 0.8×10^{-2} Scm^{-1} along ***c*** direction ($\sigma\parallel$), indicating that the preferred O^{2-} diffusion pathway is intra-layer rather than inter-layer.

Effect of A cation on ion transport. Oxide ion migration is dependent on the structural flexibility, which in turn is related to composition. Therefore, a smaller *A* cation results in greater interlayer mismatch, that is accommodated through structural modulation. By comparing Ca and Sr melilites it can be concluded that for the same concentration of interstitial oxygen, a melilite containing smaller *A* cations should yield higher ionic conductivity. Our results support this hypothesis. Thus, at the same temperature, the ionic conductivity of $[LaSr]_2[Ga]_2[Ga_2O_7]_2$ < $[NdCa]_2[Ga]_2[Ga_2O_7]_2$, $[NdSr]_2[Ga]_2[Ga_2O_7]_2$ < $[NdCa]_2[Ga]_2[Ga_2O_7]_2$, and $[La_{1.5}Sr_{0.5}][Ga]_2[Ga_2O_{7.25}]_2$ < $[La_{1.5}Ca_{0.5}][Ga]_2[Ga_2O_{7.25}]_2$ (where $R_{Nd}^{3+} < R_{La}^{3+}$, $R_{Sr}^{2+} > R_{Ca}^{2+}$) (Figure 1b and S2). Liu *et. al.*[15] similarly found that $[Nd_{1+x}Sr_{1-x}][Ga]_2[Ga_2O_{7+x/2}]_2$ (x = 0.1, 0.2) shows higher conductivity than $[La_{1+x}Sr_{1-x}][Ga]_2[Ga_2O_{7+x/2}]_2$.

Due to secondary phase formation, the conductivities of $[Nd_{1.5}Sr_{0.5}][Ga]_2[Ga_2O_{7.25}]_2$ and $[Nd_{1.5}Ca_{0.5}][Ga]_2[Ga_2O_{7.25}]_2$ do not adhere to this behavior.

Effect of interstitial oxygen on ion transport. Ionic conductivities of polycrystalline pellets of $[La_{1+x}Ca_{1-x}][Ga]_2[Ga_2O_{7+x/2}]_2$ ($0.1 \leq x \leq 0.6$) show slightly lower conductivity (0.0196 Scm^{-1} at 800°C for x = 0.5) compared to the single crystals ($\sigma\perp$ = 0.0267 Scm^{-1}), as expected due to the random orientation of grains and the influence of grain boundaries and porosity in polycrystalline pellets (Figure 1d and 1e). The conductivity increases until x = 0.5, then slightly drops when the symmetry is reduced from tetragonal to orthorhombic, and are lower than reported for the analogue $[La_{1.54}Sr_{0.46}][Ga]_2[Ga_2O_{7.27}]_2$ (0.02 ~ 0.1 Scm^{-1} at 600°C to 900°C).[7] This same study also found that $[La_{1.64}Ca_{0.36}][Ga]_2[Ga_2O_{7.32}]_2$, although exhibiting triclinic symmetry, showed high ionic conductivities comparable with the former composition at higher temperature (> 850°C) due to a phase transition to higher symmetry.[7, 16]

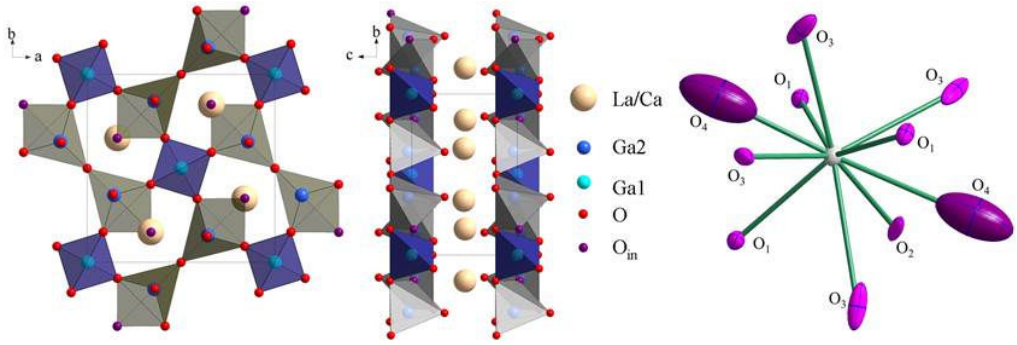

Figure 2. The structure of $[Ca_{0.5}La_{1.5}]_2[Ga]_2[Ga_2O_{7.25}]_2$ and the ten-fold AO_{10} polyhedron.

Table 1. Atomic coordinates, ADPs, bond length and angles for $[La_{1.5}Ca_{0.5}]_2[Ga]_2[Ga_2O_{7.25}]_2$ from single crystal X-ray diffraction.

Atoms	*x*	*y*	*z*	U_{iso}	Ideal occ	Refined occ
La1	0.16037(3)	0.66037(3)	0.49479(8)	0.01411(11)	0.75	0.618(3)

Ca1	0.16037(3)	0.66037(3)	0.49479(8)	0.01411(11)	0.25	0.382(3)
Ga1	0	0	0	0.01162(17)	1	1
Ga2	0.35701(5)	0.85701(5)	0.03438(11)	0.01182(12)	1	1
O1	0.3601(3)	0.8601(3)	0.6925(7)	0.0154(7)	1	1
O2	0.5	0	0.1929(12)	0.0377(18)	1	1
O3	0.0864(6)	0.1619(4)	0.7938(6)	0.0353(12)	1	1
O4	0.825(5)	0.325(5)	0.04(2)	0.12(4)	0.125	0.14(2)

Atoms	U_{11}(Å)	U_{22}(Å)	U_{33}(Å)	U_{12}(Å)	U_{13}(Å)	U_{23}(Å)
La1	0.01465(17)	0.01465(17)	0.0130(2)	-0.00327(10)	-0.00048(10)	-0.00048(10)
Ca1	0.01465(17)	0.01465(17)	0.0130(2)	-0.00327(10)	-0.00048(10)	-0.00048(10)
Ga1	0.0119(2)	0.0119(2)	0.0111(4)	0	0	0
Ga2	0.01406(19)	0.01406(19)	0.0073(3)	0.00102(17)	0.00037(13)	0.00037(13)
O1	0.0176(11)	0.0176(11)	0.0110(16)	-0.0044(16)	-0.0001(10)	-0.0001(10)
O2	0.053(3)	0.053(3)	0.007(3)	-0.041(4)	0	0
O3	0.070(3)	0.0194(16)	0.0167(15)	-0.0226(17)	0.0165(17)	-0.0061(12)
O4	0.06(2)	0.06(2)	0.25(12)	0.00(2)	-0.01(4)	-0.01(4)

Atoms	Distance (Å)	Atoms	Angle (°)
La1/Ca1-O1	2.478(3)	O3_iii(v)-Ga1-O3_iv(vi)	107.05(15)
La1/Ca1-O2	2.439(4)	O3_iii(iii, iv, iv)-Ga1-O3_v(vi, v, vi)	110.70(19)
La1/Ca1-O3	2.523(4)	O2_vii-Ga2-O1_iii	116.2(2)
La1/Ca1-O4	2.40(11)	O2_vii-Ga2-O3_i(viii)	98.71(17)
Ga1-O3	1.819(4)	O1_iii-Ga2-O3_i(viii)	119.63(14)
Ga2-O1	1.793(4)	O1_iii-Ga2-O4_ii	92(3)
Ga2-O2	1.813(3)	O3_i-Ga2-O3_viii	99.91(19)
Ga2-O3	1.853(3)	O3_i(viii)-Ga2-O4_ii	64.8(19)
Ga2-O4	2.05(4)		

Symmetry code: (i) -x,-y+1,z ; (ii) y-1,-x+1,-z+1; (iii) -y+1,x,-z+1 ; (iv) y,-x+1,-z+1 ; (v) x,y,z+1 ; (vi) -x+1/2,y+1/2,-z+1 ; (vii) -x+1,-y+1,z ; (viii) x,y-1,z ; (ix) y-1,-x,-z ; (x) -y+1,x,-z ; (xi) x,y,z-1 ; (xii) -x,-y,z-1 ; (xiii) y,-x,-z+1 ; (xiv) -y,x,-z+1 ; (xv) x,y+1,z.

Location of interstitial oxygen. Ion conduction in melilite is mediated via interstitial oxygen, which must be located experimentally to investigate the conduction mechanism. Difference Fourier maps from single crystal X-ray and neutron diffraction suggest interstitial oxygen is at the 4e Wyckoff site that is positioned within the pentagonal tunnels and at the level of gallate tetrahedral layers (Table 1 and Figure 2). In this oxygen super-stoichiometric structure, O4 is incorporated into two bonding environments such that the GaO_4 tetrahedra expand their co-ordination sphere to form distorted GaO_5 trigonal bipyramids and the La/Ca polyhedra enlarge from $(La/Ca)O_8$ to $(La/Ca)O_{10}$. In the first case, the interatomic distance of Ga-O4 is 2.05 Å, which is longer than the other tetrahedral bonds and more easily displaced, while the

O4 is stabilized by the greater electron affinity of the *A* cation, such that the La/Ca-O4 bond length is 2.40Å (typical distance of La-O is 2.441 Å and Ca-O = 2.330 Å based on the ionic radius from Shannon[17]). Including the O4, the bond valence summation (BVS) for the under-bonded La improves from 2.63 to 2.73, while the over-bonded Ga2 also increases further from 3.10 to 3.19. The contribution of O4 to the BVS for both cation species provides evidence for its incorporation into both Ga2 and La/Ca bonding environments. The atomic coordinates, bond length and angles of $[La_{1.5}Ca_{0.5}]_2[Ga]_2[Ga_2O_{7.25}]_2$ obtained from single crystal X-ray diffraction are listed in Table 1, where interstitial oxygen O4 shows a large atomic displacement parameter (ADP), and the refined composition is $[La_{1.237}Ca_{0.763}]_2[Ga]_2[Ga_2O_{7.283}]_2$.

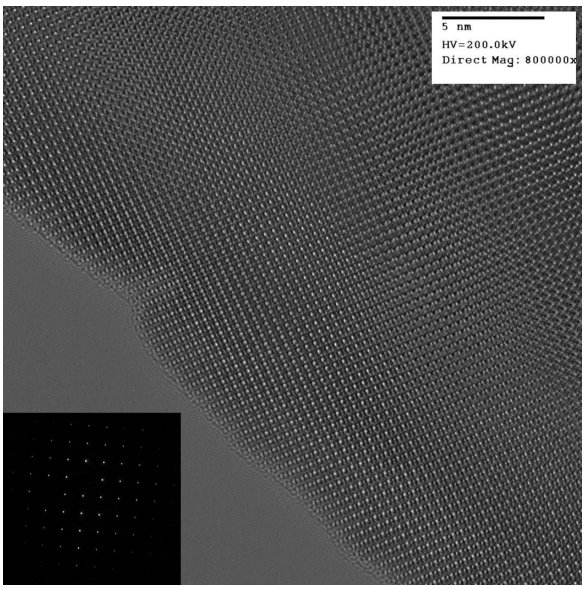

Figure 3. HRTEM image for a periodic composition ($[Ca_{0.7}Nd_{1.3}]_2[Ga]_2[Ga_2O_{7.15}]_2$) shows no structural modulation.

The stoichiometric composition $[CaLa]_2[Ga]_2[Ga_2O_7]_2$ is incommensurate,[10a] reflecting the flexible nature of the framework and its intrinsic capacity to incorporate extra-stoichiometric oxygen.[10a] As the concentration of interstitial oxygen increases, structural modulation becomes progressively less evident, until a three-dimensional (3D) structure results.[10a] Unlike

the modulated compositions which have alternate dark/bright contrast indicating modulation waves and satellites in the diffraction pattern, the HRTEM image for a 3D superstoichiometric composition (Figure 3) displays periodic lattice without modulation. This phenomenon arises because modulation provides the means to accommodate the loosely fitting *A* cation by injecting O4 into a nearby interstice that improves the BVS and reduces the need for modulation. More directly, examination of the ADPs reveals that in the modulated compositions the O4 anisotropic ellipsoids are directed towards the interlayer *A* cations.

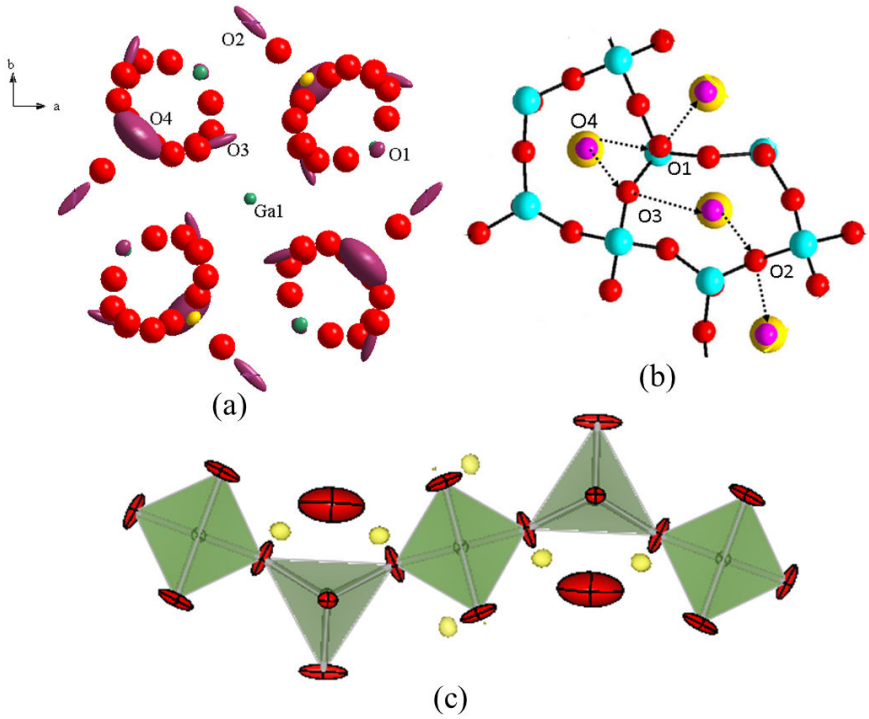

Figure 4. (a) The Fourier map with electron densities represented by red balls. (b) Schematic illustration of possible diffusion paths. The dashed lines show one of the possible diffusion paths. (c) One oxygen transport passage formed by tetrahedral network, the yellow areas are isosurface of extra electron densities.

Diffusion pathway and its crystallographic correlation. The anisotropic oxygen elongations obtained from single crystal diffraction for the superstoichiometric composition provide clear

guidance towards the intralayer diffusion paths –involving both interstitial and lattice oxygen (Figure 4a). According to the Fourier map, the oxide ion migration can occur via three paths – involving O3, O2 or O1, with the former the preferred path as shown by the relatively intense excess electron densities. This can be further verified by examining Ga-O bond length variation (Table 1), where Ga2-O3 (1.853(3) Å) and Ga1-O3 (1.819(4)Å) are longer than Ga2-O2 and Ga2-O1 with the latter the shortest (1.793(4) Å). Therefore, the bond for Ga-O3 is weak compared to the other two, and easier to break. Conversely, Ga2-O1 bond is strongest, and oxygen migration through O1 is less preferred, in agreement with the simulations of Tealdi *et. al.*.[18] Figure 4b shows the possible diffusion paths, and Figure 4c demonstrates one transport passage formed by the tetrahedral network. Molecular dynamics simulation by Tealdi *et. al.* on $[La_{1.5}Sr_{0.5}]_2[Ga]_2[Ga_2O_{7.25}]_2$ suggested a cooperative 'knock-on' diffusion mechanism,[18] where the O4 displaces the lattice oxygen to an adjacent interstitial site. This mechanism is well-accepted in many ion transport systems. For example, F^- migration in the fluorite-type structure $RbBiF_4$,[8] Li^+ cation diffusion in Li_3N,[14] and the $La_{1-x}Ba_{1+x}GaO_{4-x/2}$ perovskite electrolyte, where the oxygen vacancy is mediated by similar procedure according to the simulation of Kendrick *et. al.*.[3c] Following this mechanism, the ion transport involves breaking and reforming the Ga-O bonds, as well as the facile rotation of GaO_4 tetrahedra.

Oxygen ion transport in melilite involves facile rotation of tetrahedra that accompanies the appearance of modulation,[9, 10b] and it can be reasonably postulated that such adaptation plays a positive role in ionic migration. Further, the observation that compositions containing smaller interlayer cations give better ionic conductivities is supportive of this assumption, as stronger structural modulation can be induced by smaller interlayer cations in melilites.[10a] The incommensurate modulation is accompanied by a very flexible framework, which is the basic requirement to accommodate, relax and stabilize the interstitial defects in electrolytes.

4. Conclusions

In conclusion, anisotropic ion conduction is dominant for melilite type SOFC electrolytes, with preferred oxide diffusion within the ***ab*** plane. The ionic conductivity increases in tandem with concentration of oxygen interstitials, providing there is no symmetry reduction as lower symmetry produces more intricate diffusion paths hindering the ion transport. Moreover, the ionic conductivity also favors smaller interlayer cations. The interstitial oxygen is located inside the pentagonal rings and at the level of the tetrahedral layers. The ion transport is mediated through a cooperative 'knock-on' mechanism, which involves tetrahedral distortion and rotation, and the breaking and reforming Ga-O bonds. Combining all the results, it can be concluded that oxygen ion conduction favors those melilite compositions that display incommensurate structural modulations, which generally have smaller interlayer cations and more flexible framework.

Supporting Information

Structural information from single crystal X-ray diffraction can be obtained from the Fachinformationszentrum Karlsruhe, 76344 Eggenstein-Leopoldshafen (Germany), on quoting the depository number CSD- 428196. Electronic Supplementary Information (ESI) is available at http://www.rsc.org.

Corresponding Author

*School of Materials Science & Engineering, Nanyang Technological University, Singapore 639798.

Email: tjwhite@ntu.edu.sg

Acknowledgements

This work is funded by the Singapore MOE Tier 2 Grant (T208B1212) 'Incommensuration in Oxide Crystal Structures: Impacts on Photocatalysis and Ion Conduction', the A*STAR

(Agency for Science, Technology and Research) PSF grant no. 082 101 0021 'Optimization of Oxygen Superlattices in Solid Oxide Fuel Cell Electrolyte Apatites', and an MOE Tier 1 grant no. M52070086. The author would like to thank World Future Foundation (WFF) for the PhD prize.

1. Jacobson, A., Materials for Solid Oxide Fuel Cells. *Chem. Mater* **2010,** *22*, 660-674.
2. Garrison, E., Solid Oxide Fuel Cell. SMART.
3. (a) Islam, M. S., Ionic transport in ABO_3 perovskite oxides: a computer modelling tour. *J. Mater. Chem* **2000,** *10*, 1027-1038; (b) Yashima, M., Diffusion pathway of mobile ions and crystal structure of ionic and mixed conductors. *J. Am. Ceram. Soc* **2009,** *117*, 1055-1059; (c) Kendrick, E.; Kendrick, J.; Knight, K. S.; Islam, M. S.; Slater, P. R., Cooperative mechanisms of fast-ion conduction in gallium-based oxides with tetrahedral moieties. *Nature Mater.* **2007,** *6*, 871-875.
4. Kilo, M.; Argirusis, C.; Borchardt, G.; Jackson, R., Oxygen diffusion in yttria stabilised zirconia-experimental results and molecular dynamics calculations. *Phys. Chem. Chem. Phys* **2003,** *5*, 2219-2224.
5. An, T.; Baikie, T.; Wei, F. X.; Pramana, S.; Schreyer, M.; Piltz, R.; Shin, J.; Wei, J.; Slater, P.; White, T., Crystallographic Correlations with Anisotropic Oxide Ion Conduction in Aluminum-doped Neodymium Silicate Apatite Electrolytes. *Chem. Mater.* **2013,** *25* (7), 1109-1120.
6. Bayliss, R.; Pramana, S.; An, T.; Wei, F. X.; Kloc, C.; White, A.; Skinner, S.; White, T.; Baikie, T., Fergusonite-Type CeNbO4+δ Electrolyte: Single Crystal Growth, Symmetry Revision and Conductivity. *Journal of Solid State Chem.* **2013,** *204*, 291-297.
7. Kuang, X. J.; Green, M. A.; Niu, H. H.; Zajdel, P.; Dickinson, C.; Claridge, J. B.; Jantsky, L.; Rosseinsky, M. J., Interstitial oxide ion conductivity in the layered tetrahedral network melilite structure. *Nature Mater.* **2008,** *7*, 498-504.
8. Haering, C.; Roosen, A.; Schichl, H., Degradation of the electrical conductivity in stabilised zirconia systems: Part I: yttria-stabilised zirconia. *Solid State Ionics* **2005,** *176* (3–4), 253-259.
9. Wei, F. X.; Baikie, T.; An, T.; Schreyer, M.; Kloc, C.; White, T., Five-Dimensional Incommensurate Structure of the Melilite Electrolyte $[CaNd]_2[Ga]_2[Ga_2O_7]_2$. *J. Am. Chem. Soc.* **2011,** *133* (38), 15200-15211.
10. (a) Wei, F. X.; Baikie, T.; An, T.; Kloc, C.; Wei, J.; White, T., The crystal chemistry of melilite $[CaLa]_2[Ga]_2[Ga_2O_7]_2$: a five dimensional solid electrolyte. *Inorganic Chemistry* **2012,** *51* (10), 5941-5949; (b) Wei, F. X.; Williams, T.; An, T.; Baikie, T.; Kloc, C.; Wei, J.; White, T., Observation of atomic scale compositonal and displacive modulations in incommensurate melilite electrolyte. *Journal of Solid State Chem.* **2013,** *203*, 291-296.
11. Petricek, V.; Dusek, M.; Palatinus, L. *Jana2006. The crystallographic computing system.*, Institute of Physics, Praha, Czech Republic, 2006.
12. Keen, D. A.; Gutmann, M. J.; Wilson, C. C., *J. Appl. Crystallogr.* **2006,** *39*, 714.
13. Bruker *Topas Version 4.1*, Bruker AXS Inc.: Madison, Wisconsin, USA, 2008.
14. Li, H.; Baikie, T.; Pramana, S.; Shin, J. F.; Slater, P. R.; Brink, F.; Hester, J.; Wallwork, K.; White, T. J., Synthesis and characterisation of vanadium doped alkaline earth lanthanum gernamiate oxyapatite electrolyte. *J. Mater. Chem.* **2012,** *22*, 2658-2669.
15. Liu, B. B.; Dong, D.; Liu, Z.; Chen, F.; Xia, C., Synthesis and Electrical Conductivity of Various Melilite-type Electrolytes. *Solid State Ionics* **2011,** *191*, 68-72.

16. Li, M. R.; Kuang, X. J.; Chong, S. Y.; Xu, Z. L.; Thomas, C. I.; Niu, H. J.; Claridge, J. B.; M.J., R., Interstitial oxide ion order and conductivity in $La_{1.64}Ca_{0.36}Ga_3O_{7.32}$ melilite. *Angew. Chem. Int. Ed.* **2010,** *49*, 2362 -2366.
17. Shannon, R. D., *Acta Crystallogr. A* **1976,** *32*, 751-767.
18. Tealdi , C.; Mustarelli , P.; Islam, M. S., Layered $LaSrGa_3O_7$ -based oxide-ion conductors: cooperative transport mechanisms and flexible structures. *Adv. Funct. Mater.* **2010,** *20* (22), 3874-3880.